Optics Letters

Physical significance of backscattering phase measurements

CHENFEI HU AND GABRIEL POPESCU*

Quantitative Light Imaging Laboratory, Department of Electrical and Computer Engineering, Beckman Institute for Advanced Science and Technology, University of Illinois at Urbana-Champaign, Urbana, Illinois 61801, USA
**Corresponding author: gpopescu@illinois.edu*

Received 25 August 2017; revised 10 October 2017; accepted 11 October 2017; posted 11 October 2017 (Doc. ID 305623); published 8 November 2017

Quantitative phase imaging of transparent objects in *transmission* allows for a direct interpretation of the results: the phase shift measured is linear in the refractive index contrast and object thickness. However, the same measurement in a *backscattering* geometry yields fundamentally different results, because the incident field component is absent from the detected field. As a result, the relationship between the measured phase and object properties is obscure. We derived analytical expressions for the propagating fields under the first-order Born approximation and studied the interpretation of the measured phase shifts in backscattering versus transmission geometries. Our analysis shows that the backscattering phase shift is the result of the plane wave superposition originating at various depths in the object, which makes it impossible to infer quantitative morphology or topography information of 3D transparent samples from a reflection phase image alone.

OCIS codes: (120.5050) Phase measurement; (120.5820) Scattering measurements; (160.2710) Inhomogeneous optical media.

https://doi.org/10.1364/OL.42.004643

The phase of scattered fields is of great interest, as it carries information about the internal structure of the object under investigation [1]. To infer the structure of transparent objects, many retrieval algorithms have been applied to recover the phases from intensity-based measurements in electron microscopy, crystallography, and ptychography [2–4]. On the other hand, one can also use phase as an intrinsic contrast mechanism to image weakly absorbing samples (i.e., cells and tissues) [5]. Though most phase-imaging systems work in transmission geometry [6,7], reflection-mode platforms enable *in vivo* study or measurement of reflective surfaces [8,9].

Quantitative phase imaging (QPI) is an advanced imaging approach for mapping the phase change induced by the specimen at each point in the field of view [5]. Compared with the phase-retrieval algorithms from intensity data, which are computationally expensive and require prior assumptions on the sample to achieve uniqueness, most QPI systems recover phases uniquely from the field measured interferometrically. Recently, both transmission [10–12] and reflection [13–18] QPI systems have been developed, which enable a variety of applications [19,20]. While the interpretation of transmission QPI images is well established, to our knowledge, a physical model describing the phase image of a backscattering measurement from weakly scattering samples has not been reported.

In this Letter, we study the physical significance of the measured phase image in backscattering geometries. We start our analysis from first principles (the wave equation) and present the calculation for the reflection in close comparison with the one in transmission, pointing to both similarities and differences between the two cases. We show that, under the first-order Born approximation, the transmission phase image approaches the conventionally used expression, namely $\varphi(x,y) = \beta_0[n(x,y) - n_0]L$, with $\beta_0 = \omega/c$ being the wavenumber in vacuum, $n(x,y)$ the local refractive index, n_0 the background refractive index, and L the thickness of the specimen [Fig. 1(a)]. This linear dependence, $\varphi \propto L$, allows us to easily extract information about thickness and its fluctuations. However, the proportionality constant contains the factor $n(x,y) - n_0$ which, for live cells, is a small number of only 0.01–0.05. Thus, detecting a thickness change of δL requires detecting a pathlength change of $[n(x,y) - n_0]L$, which can be 20–100 times smaller. For a perfectly reflective sample [e.g., metal topography in Fig. 1(b)], the situation is very different. In this case, the optical pathlength difference with respect to the specularly reflected background wave is $s = 2n_0L$, which depends on L through n_0 and not n-n_0. Thus, the phase image of the reflective sample is very sensitive to thickness changes.

Nevertheless, as we demonstrate next, for a weakly scattering medium, the relationship between the measured backscattering phase images and the thickness of the object is not nearly as simple. In fact, our analysis exposes the difficulties of extracting any quantitative information about the thickness and refractive index from the measured quantitative phase image.

In order to understand the difference between the phase information extracted in reflection versus transmission, let us consider an inhomogeneous medium (e.g., tissue slice) of thickness L, as illustrated in Fig. 2.

The inhomogeneous Helmholtz equation for the total field can be written as

$$\nabla^2 U(r,\omega) + n_0^2\beta_0^2 U(r,\omega) = -\beta_0^2\chi(r,\omega)U(r,\omega), \quad (1)$$

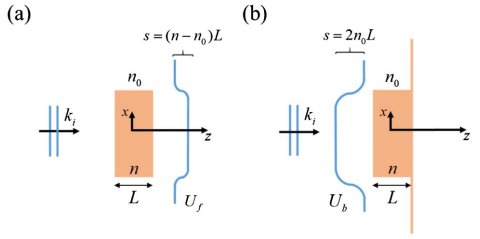

Fig. 1. Wavefront changes due to a medium of thickness L and refractive index n for (a) transmission and (b) reflection measurement. U_f and U_b denote the forward and backscattering fields, respectively.

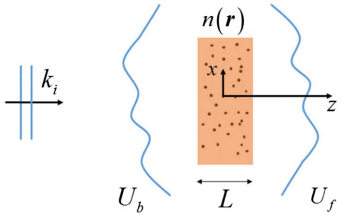

Fig. 2. Forward (U_f) and backscattering (U_b) from an inhomogeneous medium.

where U is the total field, r the spatial coordinate, ω the angular frequency, n_0 the background refractive index, $\beta_0 = \omega/c$ (with c being the speed of light in vacuum), and $\chi(r,\omega) = n^2(r,\omega) - n_0^2$ the scattering potential [21,22]. The total field is the sum between the incident field, U_0, and scattered field, U_1. As a result, Eq. (1) can be split into a *homogeneous* equation, which is satisfied by U_0, and an *inhomogeneous* one satisfied by U_1. Under the first-order Born approximation (first-order perturbation theory), we assume that the field in the medium is approximately the incident field, assumed to be a plane wave along z. Thus, we obtain

$$U_0(r,\omega) = A(\omega)e^{in_0\beta_0 z}, \tag{2}$$

$$\nabla^2 U_1(r,\omega) + n_0^2\beta_0^2 U_1(r,\omega) = -\beta_0^2\chi(r,\omega)A(\omega)e^{in_0\beta_0 z}, \tag{3}$$

where $A(\omega)$ is the spectral amplitude of the incident field, such that $A^2(\omega)$ is the power spectrum. In order to solve for the scattered field, U_1, we take the 3D Fourier transform of Eq. (3),

$$(\beta^2 - k^2)U_1(k,\omega) = -\beta_0^2 A(\omega)\chi(k_\perp, k_z - \beta, \omega). \tag{4}$$

In Eq. (4), $\beta = n_0\beta_0$, and we use the same symbols for a function and its Fourier transform but change the arguments to avoid confusion, e.g., $U_1(\boldsymbol{k},\omega)$ is the Fourier transform of $U_1(r,\omega)$ with respect to r. The right-hand side of Eq. (4) was obtained using the *shift theorem* of Fourier transforms, i.e., $f(r)e^{i\beta z} \leftrightarrow f(k_\perp, k_z - \beta)$, where f is an arbitrary signal and $\leftrightarrow$ indicates the Fourier transform operator.

From Eq. (4), we obtain right away the solution for the scattered field in the wavevector space as

$$U_1(\boldsymbol{k},\omega) = -\beta_0^2 A(\omega)\chi(k_\perp, k_z - \beta, \omega)\frac{1}{2\gamma}\left[\frac{1}{\gamma - k_z} + \frac{1}{\gamma + k_z}\right], \tag{5}$$

where $\gamma = \sqrt{\beta^2 - k_\perp^2}$. The two terms on the right-hand side correspond to the components of the scattered field that propagate along the $+z$ (forward scattering) and $-z$(backscattering). To bring Eq. (5) in the z-domain, let us take the inverse Fourier transform with respect to k_z, resulting in

$$U_1(k_\perp, z, \omega) = \left[-i\beta_0^2 A(\omega)\frac{\chi(k_\perp, z, \omega)e^{i\beta z}}{2\gamma}|_{z\geq 0}\right] \circledv_z e^{i\gamma z} + \left[i\beta_0^2 A(\omega)\frac{\chi(k_\perp, -z, \omega)e^{-i\beta z}}{2\gamma}|_{z<0}\right] \circledv_z e^{-i\gamma z}. \tag{6}$$

In Eq. (6), $\circledv_z$ indicates convolution along the z-dimension. The convolution of a function with a complex exponential results in the Fourier transform of that function multiplied by the complex exponential, namely, $e^{iqz}\circledv_z f(z) = e^{iqz}f(q)$. Combined with shift theorem, Eq. (6) can be further simplified as

$$\begin{aligned} U_1(k_\perp, z, \omega) &= -i\beta_0^2 A(\omega)\frac{e^{i\gamma z}}{2\gamma}\chi(k_\perp, \gamma - \beta, \omega)|_{z\geq 0} \\ &\quad + i\beta_0^2 A(\omega)\frac{e^{i\gamma z}}{2\gamma}\chi(k_\perp, -\gamma - \beta, \omega)|_{z<0} \\ &= U^+(k_\perp, z, \omega) + U^-(k_\perp, z, \omega). \end{aligned} \tag{7}$$

Here we use U^+ and U^- to denote, respectively, the forward and backscattering fields. Thus, the detected field in the transmission geometry is $U_f = U_0 + U^+$ [22],

$$U_f(k_\perp, z, \omega) = A(\omega)\delta(k_\perp)e^{i\beta z} - i\beta_0^2 A(\omega)\frac{e^{i\gamma z}}{2\gamma}\chi(k_\perp, \gamma - \beta, \omega). \tag{8}$$

However, the field detected in reflection does not contain the incident field. For a more straightforward comparison between the forward (U_f) and backscattering (U_b) waves, we add and subtract the incident field propagating in the $-z$ direction, to express U_b as

$$\begin{aligned} U_b(k_\perp, z, \omega) &= A(\omega)\delta(k_\perp)e^{-i\beta z} \\ &\quad + i\beta_0^2 A(\omega)\frac{e^{-i\gamma z}}{2\gamma}\chi(k_\perp, -\gamma - \beta, \omega) \\ &\quad - A(\omega)\delta(k_\perp)e^{-i\beta z}. \end{aligned} \tag{9}$$

In Eqs. (8) and (9), $\delta(k_\perp)$ indicates that the incident light is a plane wave propagating along z. Note that the $+i$ and $-i$ factors indicate a wave advanced or delayed, respectively, by $\pi/2$. In order to arrive at a physically intuitive expression for the field phase, we assume $k_\perp$ is restricted in a small region close to 0, and we can write $\gamma = \sqrt{\beta^2 - k_\perp^2} \approx \beta$. As a result, Eqs. (8) and (9) simplify to

$$U_f(k_\perp, z, \omega) = A(\omega)\delta(k_\perp)e^{i\beta z} - \frac{i}{2n_0}\beta_0 A(\omega)e^{i\beta z}\chi(k_\perp, 0, \omega), \tag{10}$$

$$U_b(k_\perp, z, \omega) = A(\omega)\delta(k_\perp)e^{-i\beta z} - A(\omega)\delta(k_\perp)e^{-i\beta z} + \frac{i}{2n_0}\beta_0 A(\omega)e^{-i\beta z}\chi(k_\perp, -2\beta, \omega). \tag{11}$$

Equations (10) and (11) emphasize another significant difference between U_f and U_b: while the former depends on the axial scattering potentials evaluated at zero (central) axial frequency, $\chi(k_\perp, 0)$, the latter depends on χ evaluated at frequency $k_z = -2\beta$. Thus, Eqs. (10) and (11) can be re-written as integrals along the z axis as

$$U_f(k_\perp,z,\omega)=A(\omega)\delta(k_\perp)e^{i\beta z}-\frac{i}{2n_0}\beta_0 A(\omega)e^{i\beta z}\int_{-L/2}^{L/2}[n^2(k_\perp,z,\omega)-n_0^2\delta(k_\perp)]e^{-ik_z z}\mathrm{d}z|_{k_z=0}, \quad (12)$$

$$U_b(k_\perp,z,\omega)=A(\omega)\delta(k_\perp)e^{-i\beta z}-A(\omega)\delta(k_\perp)e^{-i\beta z}+\frac{i}{2n_0}\beta_0 A(\omega)e^{-i\beta z}\int_{-L/2}^{L/2}[n^2(k_\perp,z,\omega)-n_0^2\delta(k_\perp)]e^{-ik_z z}\mathrm{d}z|_{k_z=-2\beta}. \quad (13)$$

The integral limits in Eqs. (12) and (13) account for the sample thickness, L. In order to predict the phase measurement in QPI, we apply the inverse Fourier transform to Eqs. (12) and (13) to bring them into the $r_\perp$ domain, namely

$$U_f(r_\perp,z,\omega)=A(\omega)e^{i\beta z}-\frac{i}{2n_0}\beta_0 A(\omega)e^{i\beta z}\int_{-L/2}^{L/2}[n^2(r_\perp,z,\omega)-n_0^2]e^{-ik_z z}\mathrm{d}z|_{k_z=0}, \quad (14)$$

$$U_b(r_\perp,z,\omega)=A(\omega)e^{-i\beta z}+\frac{i}{2n_0}\beta_0 A(\omega)e^{-i\beta z}\int_{-L/2}^{L/2}[n^2(r_\perp,z,\omega)-n_0^2]e^{-ik_z z}\mathrm{d}z|_{k_z=-2\beta}-A(\omega)e^{-i\beta z}. \quad (15)$$

If we further assume a low refractive index condition, which is justified for imaging cells and thin tissue slices, we have

$$n^2-n_0^2\approx 2n_0(n-n_0). \quad (16)$$

Using Eq. (16), we obtain simpler expressions for Eqs. (14) and (15) as

$$U_f(r_\perp,z,\omega)=A(\omega)e^{i\beta z}\{1-i\beta_0[\bar{n}(r_\perp,\omega)-n_0]L\}, \quad (17)$$

$$U_b(r_\perp,z,\omega)=A(\omega)e^{-i\beta z}\left\{1+i\beta_0\int_{-L/2}^{L/2}[n(r_\perp,z,\omega)-n_0]e^{i2\beta z}\mathrm{d}z\right\}-A(\omega)e^{-i\beta z}. \quad (18)$$

In Eq. (17), $\bar{n}(r_\perp,\omega)$ is the axially averaged refractive index, $\bar{n}(r_\perp,\omega)=\frac{1}{L}\int_{-L/2}^{L/2}n(r_\perp,z,\omega)\mathrm{d}z$. For small phase shifts, we can make the approximation $e^{ix}\approx 1+ix$, such the two fields can be expressed as

$$U_f(r_\perp,z,\omega)=A(\omega)e^{i\beta z}e^{-i\beta_0[\bar{n}(r_\perp,\omega)-n_0]L}, \quad (19)$$

$$U_b(r_\perp,z,\omega)=A(\omega)e^{-i\beta z}e^{+i\beta_0\int_{-L/2}^{L/2}[n(r_\perp,z,\omega)-n_0]e^{i2\beta z}\mathrm{d}z}-A(\omega)e^{-i\beta z}. \quad (20)$$

Equations (19) and (20) are the main result of our Letter; they show that, for weakly scattering samples, the field measured in transmission contains the conventionally defined phase term, $\varphi(x,y)=\beta_0[\bar{n}(x,y)-n_0]L$. However, the backscattering field contains the axial projection of the refractive index contrast weighted by the plane wave $e^{i2\beta z}$. Ignoring transverse features in the object, this expression indicates that the field detected in backscattering consists of a superposition of back-propagating plane waves originating at various depths, z, with respective phases $2\beta z$. This axial integral can be written in terms of a z-axis Fourier transform as

$$\phi^-(r_\perp,z)=\beta_0\int_{-\infty}^{\infty}[n(r_\perp,z,\omega)-n_0]\Pi\left(\frac{2z}{L}\right)e^{i2\beta z}\mathrm{d}z=\beta_0 L\Delta n(r_\perp,k_z,\omega)\circledv\,\mathrm{sinc}\left(\frac{Lk_z}{2}\right)|_{k_z=-2\beta}. \quad (21)$$

In Eq. (21), $\Pi(\frac{2z}{L})$ is the rectangular function of width L, $\mathrm{sinc}(x)=\sin(x)/x$, and $\circledv$ is the convolution operator in the kz domain. The phase of the scattered field depends *not* on the integral of refractive index but on its value at axial frequency -2β. Each transverse coordinate, $r_\perp$, can yield an unpredictable value at axial frequency β. The convolution with a sinc function complicates things further, as its oscillatory behavior contributes to phase shifts that vary in $x-y$ in a nontrivial manner. This result explains why quantitative phase images in backscattering are always affected by speckle, which is related to the object structure in an intricate manner. Note that even using very thin samples for which $\mathrm{sinc}(L\beta)$ approaches a constant, $\mathrm{sinc}(Lk_z/2)\approx 1$, the resulting phase, $\phi^-(r_\perp)=\beta_0 L\int\Delta n(r_\perp,k_z)\mathrm{d}k_z=\beta_0 L\Delta n(r_\perp,z=0)$, is still not the final answer. What confounds matters further is the fact that the phase imaged in backscattering is not ϕ^- but the phase of field difference, i.e., $e^{i\phi^-}-1$ according to Eq. (21). Thus, the forward and backscattering phase shifts have the form

$$\varphi_f(x,y)=\beta_0\Delta nL, \quad (22)$$

$$\varphi_b(x,y)=\arg(e^{i\phi^-}-1). \quad (23)$$

The physical significance of φ_b can be well appreciated using a phasor diagram in Fig. 3.

The two phases are related by trigonometry from Fig. 3,

$$\varphi_b\approx 90^\circ+\frac{\phi^-}{2}. \quad (24)$$

In order to illustrate the interpretation of the phase image measured in backscattering versus transmission, we performed a numerical experiment. We considered the 3D scattering potential of a live neuron measured using spatial light interference microscopy (SLIM) [12]. A stack of 70 SLIM phase map images, imaged under a 40× object (NA = 0.75), was first reconstructed and then divided by the depth of focus, assumed to be 1 μm, to yield a 3D distribution of the refractive index contrast map [Fig. 4(a)]. The method of data reconstruction is discussed in Ref. [20]. The forward [Fig. 4(b)] and backscattering phases [Fig. 4(c)] were obtained using Eqs. (23) and (24) to calculate the averaged z projection. The insets in Figs. 4(b) and 4(c) represent the zoomed-in areas of a dendrite represented by the yellow rectangle. Figure 4(c) shows both these areas next to

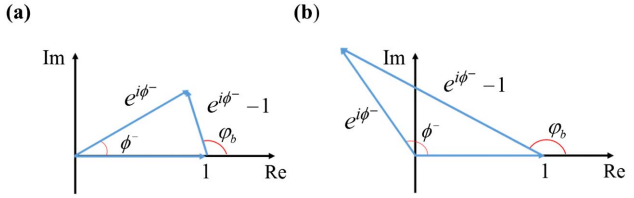

Fig. 3. Phase of backscattering field for ϕ^-(a) smaller than or (b) greater than $\pi/2$.

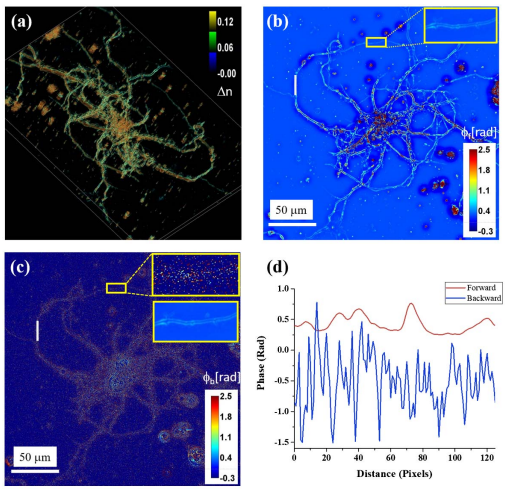

Fig. 4. Comparison of measured phase image of transmission versus backscattering field. (a) 3D refractive index contrast map is obtained from SLIM images divided by the depth of focus of 1 μm. The simulated (b) forward and (c) backscattering phase (unit in radians) were then calculated following the equations described in the paper. (d) Phase values along the white solid lines in (b) and (c).

each other, demonstrating how vastly different the forward and backscattering phase measurements of the same cell region are. Furthermore, Fig. 4(d) plots the phase values along the same length of a dendrite, indicated by the white solid lines in Figs. 4(b) and 4(c). Clearly, the two signals are completely different. Note that, while it is true that the backscattering measurement consists of higher spatial frequencies from the object, the backscattering phase is not simply the high-pass version of the transmission phase. These results make it apparent that the phase signals obtained in backscattering and their statistics cannot be immediately related to the object structure. In fact, the backscattering phase maps appear as random speckle patterns. The contour of the object can be identified from the background only because the speckle statistics are different from those of the background.

In summary, while in transmission we recover the well-known formula that relates linearly the phase to the object thickness and refractive index contrast, the situation in backscattering is much more complicated. The fundamental difference is that the *momentum transfer* (or scattering wavevector) has zero average in transmission, but approaches 2β in reflection. In other words, the backscattering field contains high spatial frequencies due to the superposition of plane waves backscattered from various depths in the object. The relationship between the phase, thickness, and refractive index of the object is completely obscured, and the phase map is a speckle distribution. The interpretation for weakly scattering media suggests that, for strongly scattering media, the problem only becomes more difficult. Finally, another way to paint an intuitive picture of this result is to consider the spatial correlation of the forward versus backscattering field. Under plane wave illumination, which is completely spatially correlated, the forward field remains quasi-correlated because the incident field is dominant, i.e., the spatial spectrum broadening is negligible for light transmitted by transparent objects. On the other hand, the backscattered field has no dominant k-vector, the incident field is missing, and the broad spatial spectrum translates into a narrow spatial correlation area. It is not surprising then that the phase shift values are not well correlated across the field of view and, in fact, approach a random speckle pattern. Finally, we believe that our formalism will apply to a confocal geometry as well, provided the illumination field is now expressed as a superposition of plane waves. While we showed that the scattering problem in a confocal geometry has an analytic solution under the first-order Born approximation [23], deriving the phase image formula is left for a separate publication.

Funding. National Science Foundation (NSF) (0939511, 1353368, 1450962).

REFERENCES

1. E. Wolf, *Advances in Imaging and Electron Physics*, P. W. E. Hawkes, ed. (Academic, 2011).
2. J. R. Fienup, Appl. Opt. **21**, 2758 (1982).
3. G. A. Zheng, R. Horstmeyer, and C. H. Yang, Nat. Photonics **7**, 739 (2013).
4. B. S. Zhang, D. F. Gardner, M. D. Seaberg, E. R. Shanblatt, H. C. Kapteyn, M. M. Murnane, and D. E. Adams, Ultramicroscopy **158**, 98 (2015).
5. G. Popescu, *Quantitative Phase Imaging of Cells and Tissues*, McGraw-Hill Biophotonics (McGraw-Hill, 2011), p. 362.
6. F. Zernike, Physica **9**, 686 (1942).
7. G. Nomarski, J. Phys. Radium **16**, 9S (1955).
8. T. N. Ford, K. K. Chu, and J. Mertz, Nat. Methods **9**, 1195 (2012).
9. K. A. Goldberg and I. Mochi, J. Vac. Sci. Technol. B **28**, C6e1 (2010).
10. B. Bhaduri, C. Edwards, H. Pham, R. J. Zhou, T. H. Nguyen, L. L. Goddard, and G. Popescu, Adv. Opt. Photon. **6**, 57 (2014).
11. P. Marquet, B. Rappaz, P. J. Magistretti, E. Cuche, Y. Emery, T. Colomb, and C. Depeursinge, Opt. Lett. **30**, 468 (2005).
12. Z. Wang, L. Millet, M. Mir, H. F. Ding, S. Unarunotai, J. Rogers, M. U. Gillette, and G. Popescu, Opt. Express **19**, 1016 (2011).
13. Y. Choi, P. Hosseini, W. Choi, R. R. Dasari, P. T. So, and Z. Yaqoob, Opt. Lett. **39**, 6062 (2014).
14. R. J. Zhou, D. Jin, P. Hosseini, V. R. Singh, Y. H. Kim, C. F. Kuang, R. R. Dasari, Z. Yaqoob, and P. T. C. So, Opt. Express **25**, 130 (2017).
15. G. Maire, F. Drsek, J. Girard, H. Giovannini, A. Talneau, D. Konan, K. Belkebir, P. C. Chaumet, and A. Sentenac, Phys. Rev. Lett. **102**, 213905 (2009).
16. T. Yamauchi, H. Iwai, M. Miwa, and Y. Yamashita, Opt. Express **16**, 12227 (2008).
17. K. Belkebir and A. Sentenac, J. Opt. Soc. Am. A **20**, 1223 (2003).
18. E. Mudry, P. C. Chaumet, K. Belkebir, G. Maire, and A. Sentenac, Opt. Lett. **35**, 1857 (2010).
19. Y. Park, M. Diez-Silva, G. Popescu, G. Lykotrafitis, W. Choi, M. S. Feld, and S. Suresh, Proc. Natl. Acad. Sci. USA **105**, 13730 (2008).
20. K. Lee, K. Kim, J. Jung, J. Heo, S. Cho, S. Lee, G. Chang, Y. Jo, H. Park, and Y. Park, Sensors **13**, 4170 (2013).
21. M. Born and E. Wolf, *Principles of Optics: Electromagnetic Theory of Propagation, Interference and Diffraction of Light* (Elsevier, 2013).
22. T. Kim, R. J. Zhou, L. L. Goddard, and G. Popescu, Laser Photon. Rev. **10**, 13 (2016).
23. T. Kim, R. Y. Zhu, T. H. Nguyen, R. J. Zhou, C. Edwards, L. L. Goddard, and G. Popescu, Opt. Express **21**, 20806 (2013).